SYNTHESIS, STRUCTURAL AND OPTICAL PROPERTIES OF Zn-SUBSTITUTED Co W-FERRITES BY COPRECIPITATION METHOD

N. AMIN[a], M. AKHTAR[a], M. SABIR[a], K. MAHMOOD[a], A. ALI[a], G. MUSTAFA[b], M. S. HASAN[c], A. BIBI[d], M. Z. IQBAL[e], F. IQBAL[f], A. REHMAN[a], A. ASLAM[a], K. MEHMOOD[a], Z. LATIF[a], K. HUSSAIN[a], Z.H. NAWAZ[a], M. FATIMA[a] S. NADEEM[a], S. SHARIF[a], M. JILANI[a], A. GHAFFAR[a], K. JAVEED[a], R. ZAKIR[e], A. AMEEN[g], M. I. ARSHAD[a,*]

[a]*Department of Physics, Government College University, Faisalabad 38000, Pakistan*

[b]*Department of Physics, Bahauddin, Zakariya University Multan, 60800, Pakistan*

[c]*Department of Physics, The University of Lahore, 1-kM Raiwind Road, Lahore, Pakistan*

[d]*Laboratory of NBA, Jiangsu Key Laboratory for CBFMD, Institute of FNSM and Collaborative Innovation Center of SNT, Soochow University, Suzhou, Jiangsu 215123, China*

[e]*Nanotechnology Research Laboratory, GIK Institute of Engineering Science and Technology, Topi 23640, Khyber Pakhtunkhwa, Pakistan*

[f]*Depaartment of Physics, The Islamia university of Bahawalpur, Bahawalpur, Pakistan.*

[g]*Department of Physics, University of Agriculture Faisalabad, Faisalabad, Pakistan.*

A series W-type $BaMe_2Fe_{16}O_{27}$ ferrites withcomposition $BaZn_xCo_{1-x}Fe_{16}O_{27}$(x = 0.0, 0.1, 0.2, 0.3, 0.4 &0.5) were manufactured by co-precipitation method sintering at 1100°C for 8 h. XRD, FTIR, SEM, UV-vis and I-V techniques were applied to investigate structural, optical, morphological and electrical properties respectively. Crystallite size was observed in the range of (37.58 nm- 54.75 nm) revealed by XRD and was confirmed by SEM analysis. IR exposed the existence of metal oxides (M -O). Optical band gap was in (3.0 eV- 5.2 eV) range which proved the trend of DC resistivity in increasing trend. Activation energy discovered the conversion of ferrimagnetism to paramagnetism characteristics confirming the W-type materials are highly suitable for novel application.

(Received August 6, 2019; Accepted January 7, 2020)

Keywords: Hard ferrites, Co-precipitation, XRD and UV-vis, DC resistivity

1. Introduction

Barium base W-type ferrites with composition $BaZn_xCo_{1-x}Fe_{16}O_{27}$are an interesting class of ferromagnetic oxides. In hexagonal organization $Fe^{+3}$are distributed in 5 distinct crystallographic locations, one tetrahedral ($4f_1$), 3 octahedral (2a,12k and $4f_2$) and one trigonal bipyramidal (2b) sites. In Ba hexaferrites, along crystallographic c-axis spins of three sites 12k, 2b and 2a sites are aligned and parallel to each other when in the magnetically ordered state while spins of $4f_2$ and $4f_1$ sites spots in the contradictory direction. By considering number of diamagnetic and paramagnetic cations belongings on the magnetic belongings of Zn^{+2} replacement Ba-Co W-type ferrites are one of the most imperative work allied with exercise of these nanomaterials in mixture of modern technological relevance [1]. As of stronger resistivity, power other including eddy current losses and decreased astonishingly and make the produce ferrite materials more suitable in high frequency device fabrications [2, 3]. Several techniques have been

* Corresponding author: miarshadgcuf@gmail.com

developed and effectively employed for synthesis of ferrites like ceramic system [3-4], solution combustion performance [5], sol-gel auto combustion route [6], ball milling [7] and co-precipitation procedure [8]. In current research work, we have stated the separation of $BaZn_xCo_{1-x}Fe_{16}O_{27}$(x = 0.0-0.5 with step interval 0.1) ferrites byco-precipitation method. In addition to that, the influence of Zn^{+2} concentrations on the structural and optical traits of $BaZn_xCo_{1-x}Fe_{16}O_{27}$ nanomaterials were scrutinized.

2. Experimental procedure

Present research work is to synthesize and to study the characterizations of $BaZn_xCo_{1-x}Fe_{16}O_{27}$with x = 0.0, 0.1, 0.2, 0.3, 0.4 & 0.5ferrites by co-precipitation technique. Needed compositions $BaZn_xCo_{1-x}Fe_{16}O_{27}$ were attained using stoichiometric proportions of $Ba(NO_3)_2.6H_2O$, $Co(NO_3)_2.6H_2O$, $Zn(NO_3)_3.6H_2O$, $Fe(NO_3)_3.9H_2O$ and NaOH. They were dissolved in deionized water. NaOH solution was used as precipitant. pH of solution was maintained 11 and was stirred for the period of 1 h at magnetic stirrer. Resulted precipitates were digested in a preheated water bath at 80 ^oC for 30 min duration. In order to make the precipitates free of impurities they were washed with deionized water many times. Obtained products were desiccated at 90 °C temperatures in an oven for 12 h to get rid of water contents.

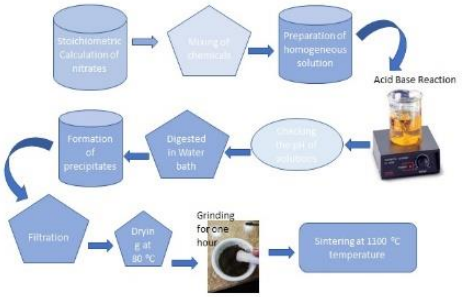

Fig. 1. Flow chart for $BaZn_xCo_{1-x}Fe_{16}O_{27}$with x = 0.0, 0.1, 0.2, 0.3, 0.4 & 0.5.

Mortar and pestle were employed to grind the materials into fine powder then sintered at 1100°C for 8 h. After again grinding of each fabricated nanoferrite sample for the period of 30 mint samples were sent for the characterizations including XRD, FTIR SEM and I-V. Fig. 1 shows the flow chart of entire methodology.

3. Result and discussion

3.1 Microstructural study

X-ray diffraction (XRD) peaks patterns were gained at room temperature by the application of powder samples in an Xpert Pro panalytical diffract meter with copper K-alpha radiation (λ = 1.54056 Å) at 40 kilo Volt and 30 mili Ampere current. Data amongst intensity and 2-theta were composed by step counting routine with 0.05°/s scanning speed and 20 - 60° range of 2-theta. Fig. 2 shows the X-ray diffraction models of W-type ferrites Ba $Zn_xCo_{1-x}Fe_{16}O_{27}$with concentration (x = 0.0, 0.1, 0.2, 0.3, 0.4 & 0.5) nanoparticles. XRD data confirmed the formation of W type Ba substituted Zn-Co hexagonal ferrites. Prominent peaks are shown in Fig. 2 (b) of all hexagonal ferrites while Fig. 2 (a) displays hexagonal structure of W-type ferrites for all samples. XRD data was used to calculate the structural factors including lattice parameters (‘a’ and ‘c’) and size of particle (D) of W-type ferrites using the following formula [9],

$$\mathrm{Sin}\theta^2 = \mathrm{A}\,(h^2 + hk + k^2) + \mathrm{C}\,l^2 \quad (1)$$

A and C were computed through the following equations as,

$$A = \frac{\lambda^2}{3a^2} \tag{2}$$

$$C = \frac{\lambda^2}{4c^2} \tag{3}$$

where 'a' and 'c' indicate lattice constant, (h k l) denotes Miller indices and Scherer's formula ascribed by equations (1 – 3). From equations (2) and (3) c/a ratio was attained [10]. Lattice parameter ratios show that they are variables. Such variations are because of diversities in ionic radii of Zn^{2+} (0.74 A°) and Co^{2+} (0.72 A°). Fig. 3 illustrates the plot between lattice constant ratio and concentration. Scherrer's principle was utilized to calculate the crystallite size D as,

$$D = \frac{k\lambda}{B_{(hkl)}\cos\theta} \tag{4}$$

where, K represents shape aspect, λ indicates X-ray wavelength (1.54 A°), θ specifies Bragg's diffraction angle and $B_{hkl}$is full width and half maximum (FWHM). Crystallite size has the range of 37.58 nm- 54.75 nm as in table 1. Fig. 4 shows the relation among crystallite size and concentration. From Fig. 4, it can be investigated that crystallite has variations with the addition of Zn^{2+} contents. Initially crystallite size increases to maximum value of 54.75 nm for X = 0.0 to 0.2 and then shows lowest value of 24.1 nm for X = 0.3 then again, some extent increases for X = 0.4 and then again demonstrates lower values for X = 0.5. Such discontinuous performance is attributed to the increase of Zn^{2+} contents and decease of Co^{2+} contents.

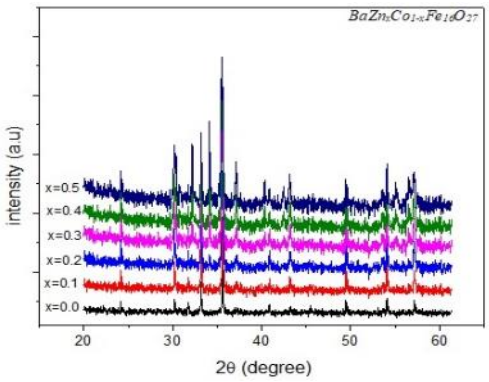

Fig. 2. (a, b). XRD Patterns of $BaZn_xCo_{1-x}Fe_{16}O_{27}$(x = 0.0-0.5) ferrites.

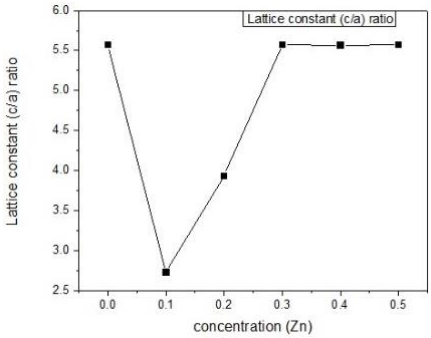

Fig. 3. Plot of lattice constant ratio (c/a) and concentration (Zn).

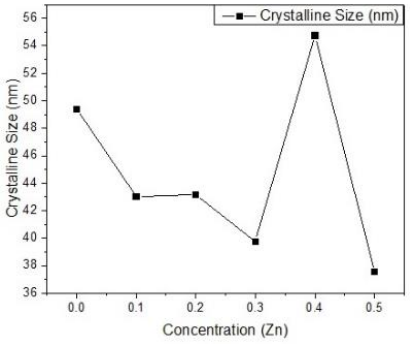

Fig. 4. Plot of crystallite size and concentration (Zn).

Table 1. Compositions, lattice constant, crystallite size, resistivity and activation energy of $BaZn_xCo_{1-x}Fe_{16}O_{27}$ *(x = 0.0-0.5) hexaferrites.*

Composition (X)	Lattice constant (A^o)	Crystallite size (nm)	Resistivity (Ω-cm)×10^9	Activation Energy (ev)
$BaCo_1Zn_0Fe_{16}O_{27}$	5.02656	49.38552	2	0.0212
$BaCo_{0.9}Zn_{0.1}Fe_{16}O_{27}$	5.03203	43.02694	1.5	0.0359
$BaCo_{0.8}Zn_{0.2}Fe_{16}O_{27}$	5.03882	43.17667	3	0.029
$BaCo_{0.7}Zn_{0.3}Fe_{16}O_{27}$	5.04316	39.72201	2.5	0.012
$BaCo_{0.6}Zn_{0.4}Fe_{16}O_{27}$	5.24679	54.75247	3.5	0.01931
$BaCo_{0.5}Zn_{0.5}Fe_{16}O_{27}$	5.05155	37.58228	4	0.01514

3.2. FTIR Spectroscopy

FTIR spectra for Zn^{2+} doped hexaferrites annealed at 1100 °C are given in Fig. 5. 400cm^{-1} - 4000 cm^{-1} spectrum was adjusted to exhibit absorption peaks. Lower frequency band (V_2) and upper frequency band (V_1) is observed through this information. Upper frequency band also called intrinsic vibrations of tetrahedral frequency band. Tetrahedral frequency band range was noted in order of 400 cm^{-1} – 600 cm^{-1}. Existence of such frequency group ensured the presence of metal oxides (M – O) [11].

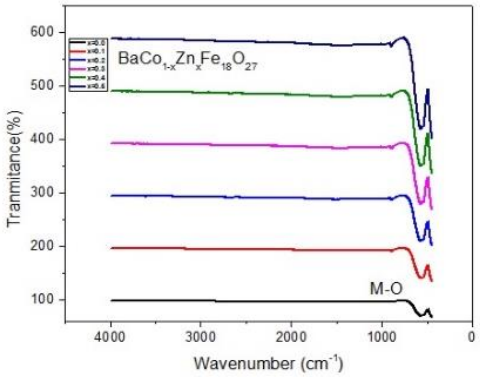

Fig. 5. FITR pattern Ba $Zn_xCo_{1-x}Fe_{16}O_{27}$*(x = 0.0, 0.1, 0.2, 0.3, 0.4 & 0.5) ferrites.*

3.3. Morphological Analysis

Facade morphology and microstructure of hexaferrites were deliberated by JSM-6490 JEOL scanning electron microscope (SEM). Scanning electron microscopy (SEM) method was applied to examine morphological analysis of zinc inserted hexferrites. Fig. 6 gives the micro image of presented sample. SEM image confirms the particle size obtained from the XRD analysis. SEM micro graphs confirms that W-ferrites are in organized structures. It seems that

inhomogeneous grain size shows hexagonal pale let shapes. Same kinds of structures were obtained for rest of nanomaterials [12].

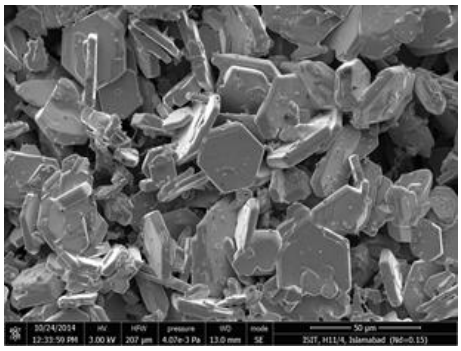

Fig. 6. SEM micrographs $BaZn_xCo_{1-x}Fe_{16}O_{27}$ferrites.

3.4. Optical Properties

UV-visible absorption spectrums were traced by application of UV-vis-NIR spectrophotometer (Perkin Elmer Lambda 9). Investigation of optical assets of light including absorption, reflection, transmission at room temperature and band gap energy is of an immense significance in optoelectronics relevance. Fig. 7 illustrates that absorbance variation for Zn^{+2} substituted Co W ferrites as the function of wavelength. The sharp peaks appeared in near ultra violet visible spectrum indicate that the colloid is splendid dispersing. Fig. 7 shows the (%A) conduct improve concentration of Zn^{+2} are increased from x = 0.0 to x = 0.5. The desired band gaps obtained for all samples are shown in Fig. 8 (a-b) also considered by Tauc's equation as [3],

$$\alpha hv = A(hv - E_g)^n \tag{5}$$

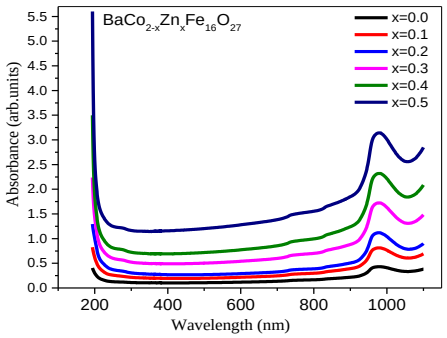

Fig.7. Spectral absorbance of $BaZn_xCo_{1-x}Fe_{16}O_{27}$ ($x = 0.0$- 0.5) ferrites.

Here E_g represents optical band gap, hv indicates photon energy, A is constant depending on the transition prospect, α is coefficient of absorption and n indicates ½ or 2 for direct or indirect energy bandgap for hexaferrites material. Coefficient of absorption (α) can be intended using this relation,

$$\alpha = \frac{4\pi k}{\lambda} \tag{6}$$

where in above mentioned equation (6) k is index of absorption and λ is wavelength (nm). Calculated values of optical bandgap energy (E_g) of all investigated samples are measured by design of Tauc's diagram between $(\alpha hv)^2$ against (hv) energy of photons as shown in Fig. 8 (a-

b). Band gap energy is illustrated by the intercept of linear section on x-axis at $(\alpha hv)^2$ related to zero. Investigated experiential bandgap energy measurements are established in the range (3.0 eV to 5.2 eV) of w-type ferrites. Imperfections in lattice, different position of atoms and grain boundary diffusions are major issues [13]. It can also be revealed that energy band gap boosts up with the declination of grain size.

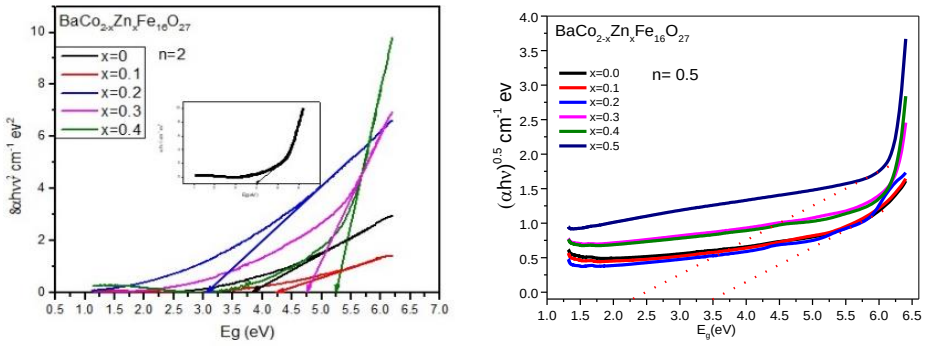

Fig. 8. Plot $(\alpha hv)^{1/2}$ versus $E_g(ev)$ at (a) n=2 and (b) n= 0.5.

3.5. I-V Characterizations

For Zn^{+2} substitution of $BaZn_xCo_{1-x}Fe_{16}O_{27}$ferrites with (I-V) were examined by using Keithley electrometer model 2401. I-V graph gives the curve data of following samples as shown in Fig. 9. Resistivity of ferrites can be investigated through the following equation as,

$$\rho = \frac{RA}{L} \tag{7}$$

$$R = \frac{1}{slope} \tag{8}$$

where, L = thickness of prepared pellets, A = area of electrode in contact with the sample [14]. The measured electrical resistivity for presented sample with Zn^{+2} contents are listed in Table 2. Tabulated data shown the resistivity of prepared samples with the increase of temperature. Temperature was increased with the difference of 50 $^{\circ}$C up to 550 $^{\circ}$C. The studied results uncovered that electrical resistivity was amplified with Zn^{+2} contents. Fig 9 gives the relation between temperature and resistivity. It can be observed that resistivity is growing continuously with the rise in temperature. It is because of increase in distance between valance band and conduction band i.e., band gap energy illustrated in Fig. 8 (b). Same kind of behavior is shown by rest of hexaferrites nanoparticles. Fig. 10 shows such kinds of trends amongst resistivity and concentration for $BaZn_xCo_{1-x}Fe_{16}O_{27}$ (X = 0.0 – 0.5) ferrites. It can be revealed that resistivity is developing with the increase of Zn^{2+}concentration [15]. Resistivity is increasing in the range of 1.5 x 10^9 – 4 x 10^9 ohm-cm as in table 1. The temperature at which materials change properties from ferrimagnetism to paramagnetism is call curie temperature. Energy required the material to change the properties is called activation energy. Activation energy for all Zn doped Co-W ferrites is shown in the Fig. 11. Such kinds of materials are highly applicable in recording media devices [16].

Table 2. Temperature and resistivity for presented sample of $BaZn_xCo_{1-x}Fe_{16}O_{27}$ (X = 0.0 – 0.5) ferrites.

Temperature (°C)	$\rho \times 10^9$ (ohm-cm)
50	0.8
100	0.9
150	1.3
200	1.5
250	1.8
300	2
350	2.7
400	3
450	3.1
500	3.4
550	4

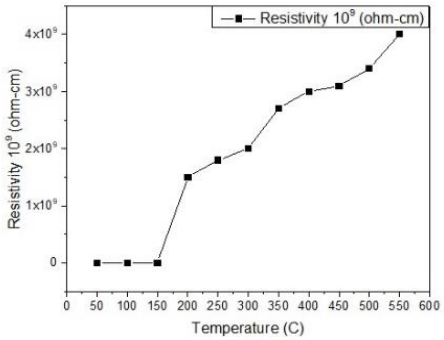

Fig. 9. Relation between temperature and resistivity for presented sample of $BaZn_xCo_{1-x}Fe_{16}O_{27}$ (X = 0.0 – 0.5) ferrites.

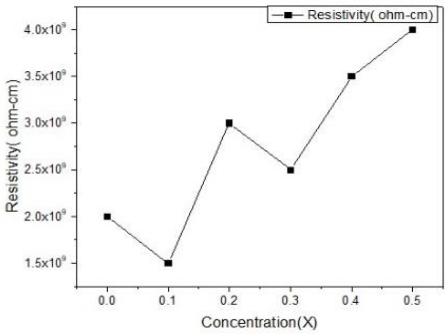

Fig. 10. Variation of resistivity versus contents (x).

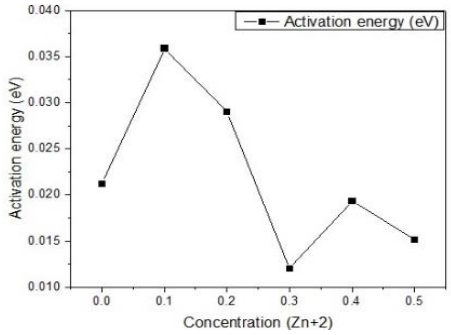

Fig. 11. Plot of activation energy and concentration (Zn^{2+}).

4. Conclusions

A series W-type $BaMe_2Fe_{16}O_{27}$ ferrites with composition $BaZn_xCo_{1-x}Fe_{16}O_{27}$ (x = 0.0, 0.1, 0.2, 0.3, 0.4 & 0.5) were manfactured by co-precipitation process sintering at 1100 °C for 8 h. Structural, optical, morphological and electrical properties were investigated. Crystallite size was observed in the range of 37.52 nm- 54.75 nm revealed by XRD and was confirmed by SEM analysis. Existence of metal oxides (M - O) group was confirmed by FTIR. Optical band gap was in 3.0 eV -5.2 eV range which proved the trend of DC resistivity in increasing trend. Activation energy results trend describe that the conversion of ferrimagnetism to paramagnetism characteristics confirming the W-type materials are highly suitable for novel application.

Acknowledgements

The author is thankful to Higher Education Commission (HEC) of Pakistan for contributing financial support in completing this work under IRSIP scholarship.

References

[1] A. K.Nikumbh et al., Journal of Alloys and Compounds **683**, 346 (2016).
[2] S. Rohit, T. Prashan, K. Manoj, S. Pankaj, S. Vineet, Journal of Alloys and Compounds **704**, 7 (2018).
[3] M. S. Hasan et al., Journal of Materials Research Express **6**, 1 (2018).
[4] S. R. Bhongale et al., Journal of Magnetism and Magnetic Materials **441**, 475 (2017).
[5] P. P. Hankare et al., Journal of Materials Compounds **485**, 798 (2009).
[6] M. George, M. A. John, S. S. Nair, P. A. Joy, M. R. Anantharaman, Journal of Magnetism and Magnetic Materials **302**, 190 (2006).
[7] K. O. Ukoba, Q. Eboka, F. L. Inambao, Journal of Renewable and Sustainable Energy **82**, 2900 (2018).
[8] M. T. Hammad, K. J. Salem, A. A. Amsha, N. Hejazy, Journal of Materials Compounds **741**, 123 (2018).
[9] F. Lv et al., Journal of Materials Letter **157**, 277 (2015)
[10] X. Niu et al., Journal of Optik **126** (24), 5513 (2015).
[11] A. Shitre et al., Materials Letters **56** (3), 188 (2002).
[12] M. J. Iqbal et al., Materials Research Bulletin **46** (11), 1980 (2011).
[13] N. F. Djaja et al., Advances in Materials Physics and Chemistry **3**(01), 33 (2013).
[14] N. Amin et al., Journal of Digest Journal of Nanomaterials and Biomaterials **14** (2), 501 (2019).
[15] A. K. Nikumbh et al., Journal of Alloys and Compounds **683**, 346 (2016).
[16] A. Verma et al., Materials Science and Engineering: B **116**(1), 1 (2005).